Epithelial control of colonisation by *Streptococcus pneumoniae* at the human mucosal surface

Caroline M Weight[1], Cristina Venturini[1], Sherin Pojar[2], Simon P. Jochems[2], Jesús Reiné[2], Elissavet Nikolaou[2], Carla Solorzano[2], Carl Anderson[3], Mahdad Noursadeghi[1], Jeremy S Brown[4], Daniela M. Ferreira[2], Robert S Heyderman[1]

[1]Division of Infection and Immunity, University College London, London, United Kingdom, [2]Department of Clinical Sciences, Liverpool School of Tropical Medicine, Liverpool, United Kingdom, [3]Wellcome Sanger Institute, Hinxton, [4]Department of Respiratory Medicine, University College London, London, United Kingdom

Corresponding Author: Dr Caroline M. Weight, Division of Infection and Immunity, Cruciform Building, Gower Street, University College London, WC1E 6BT, UK. Email: c.weight@ucl.ac.uk; Tel: 02031082127

Abstract

Control of *Streptococcus pneumoniae* colonisation at human mucosal surfaces is critical to reducing the burden of pneumonia and invasive disease, interrupting onward transmission, and in achieving herd protection. We hypothesised that the pattern of pneumococcal-epithelial engagement dictates the inflammatory response to colonisation, and that this epithelial sensing is linked to bacterial clearance. Here we have used nasal curette biopsies from a serotype 6B Experimental Human Pneumococcal Carriage Model (EHPC) to visualize *S. pneumoniae* colonisation and relate these interactions to epithelial surface marker expression and transcriptomic profile upregulation. We have used a Detroit 562 cell co-culture model to further understand these processes and develop an integrated epithelial transcriptomic module to interrogate gene expression in the EHPC model. We have shown for the first time that pneumococcal colonisation in humans is characterised by microcolony formation at the epithelial surface, microinvasion, cell junction protein association, epithelial sensing, and both epithelial endocytosis and paracellular transmigration. Comparisons with other clinical strains *in vitro* has revealed that the degree of pneumococcal epithelial surface adherence and microinvasion determines the host cell surface marker expression (ICAM-1 and CD107), cytokine production (IL-6, IL-8 and ICAM-1) and the transcriptomic response. In the context of retained barrier function, epithelial microinvasion is associated with the upregulation of a wide range of epithelial innate signalling and regulatory pathways, inflammatory mediators, adhesion molecules, cellular metabolism and stress response genes. The prominence of epithelial TLR4R signalling pathways implicates pneumolysin, a key virulence factor, but although pneumolysin gene deletion partially ameliorates the inflammatory transcriptional response *in vitro*, critical inflammatory pathways persist in association with enhanced epithelial adhesion and microinvasion. Importantly, the pattern of the host-bacterial interaction seen with the 6B strain *in vitro* is also reflected in the EHPC model, with evidence of microinvasion and a relatively silent epithelial transcriptomic profile

that becomes most prominent around the time of bacterial clearance. Together these data suggest that epithelial sensing of the pneumococcus during colonisation in humans is enhanced by microinvasion, resulting in innate epithelial responses that are associated with bacterial clearance.

Keywords

Streptococcus pneumoniae, mucosa, Innate cell response, Epithelial cells, host-pathogen interactions, Human Challenge Model, RNA sequencing

Highlights

- Colonisation of the human mucosa by *Streptococcus pneumoniae* is associated with microcolony formation, microinvasion, epithelial sensing and an epithelial innate response.
- Following adherence to the epithelial cell surface, microinvasion of the epithelium may occur by endocytosis and/or lateral migration between cells without necessarily compromising barrier integrity.
- The pattern of pneumococcal epithelial surface adherence and microinvasion determines the host cell response through a range of innate signaling and regulatory pathways, inflammatory mediators, adhesion molecules, cellular metabolism and stress response genes.
- Epithelial sensing is triggered by, but not wholly dependent on pneumolysin, a key virulence factor of *S. pneumoniae*.

Introduction

Colonisation of upper respiratory tract (URT) mucosa by a range of bacteria is a necessary precursor to transmission and disease. *Streptococcus pneumoniae* is a common coloniser of the human nasopharynx and is estimated to be responsible for >500,000 deaths due to pneumonia, meningitis and bacteraemia in children aged 1–59 months worldwide[1]. In comparison to gut pathogen-mucosal interactions[2], the control of pneumococcal colonisation is far less well understood, particularly in humans[3].

In Europe and North America, there has been a dramatic impact of pneumococcal conjugate vaccine (PCV) on vaccine serotype (VT) invasive disease and carriage[4,5]. Indeed, more than 50% of PCV impact has been due to a reduction in VT colonisation resulting in reduced transmission and therefore disease. This is the basis of herd protection[4,5]. However, the emergence of non-VT pneumococcal disease across the world and the more modest impact of PCV on colonisation in high transmission settings threaten this success[6-10]. As a first step towards further optimising vaccine impact on pneumococcal colonisation, it is critically important to define the mechanistic basis of the control of *S. pneumoniae* at the mucosal surface.

We and others have previously demonstrated that antigen-specific URT mucosal T cell immune memory to subcapsular pneumococcal protein antigens in humans is acquired with age in humans, is predominately pro-inflammatory and is heavily regulated by Treg[11-13]. Antibodies to subcapsular protein antigens rather than to the polysaccharide capsule (the target of currently licenced vaccines), also appear important for the natural control of colonisation and clearance[14]. We and others[15,16], suggest that the URT epithelium is at the centre of this process, orchestrating both innate/inflammatory and adaptive immune mechanisms[17-19], promoting bacterial clearance. The epithelium senses bacteria colonising the mucosal surface, rapidly transducing inflammatory signals and recruiting immune cells. However, murine models[20] and epidemiological studies of viral-

coinfection[21,22] suggest that the resulting inflammation also leads to onward transmission to susceptible individuals[23]. This inflammation-driven transmission is crucial for the continued success of the pneumococcus.

Nasal colonisation by *S. pneumoniae* in murine models is proinflammatory[24] and is associated with epithelial paracellular transmigration and tight junction modulation[25]. Mediated though pneumococcal protein C (PspC)–polymeric immunoglobulin receptor (pIgR) interactions[26,27], *S. pneumoniae* invasion of immortalised epithelial cell monolayers has also been shown to occur by endocytosis[27]. The relative importance of epithelial endocytosis and paracellular migration in microinvasion remains uncertain[27] but may influence epithelial sensing of this otherwise extracellular pathogen through multiple pathogen-associated molecular patterns (PAMPS). These may include TLR2 signalling via lipoteichoic acid[28], Nod1 signalling via peptidoglycan[29] and TLR4 signalling via pneumolysin[23,30], a pore-forming toxin that mediates transmission in an infant mouse model[23,30]. Indeed, microinvasion of the epithelium may overcome the sequestering of pattern recognition receptors either at the basolateral surface or intracellularly[31-33].

Much of what we understand of the control of pneumococcal colonisation is derived from epidemiological studies and murine carriage models. Experimental human pneumococcal challenge (EHPC) model provides a well-controlled, reproducible tool to characterise the cellular and molecular mechanisms that underlie pneumococcal colonisation in humans[34]. We have therefore explored the hypothesis that epithelial microinvasion by *S. pneumoniae* enhances the innate immune responses associated with colonisation and have characterised the underlying cellular and molecular mechanism. Here, we show that pneumococcal colonisation in humans is characterised by microcolony formation and junctional protein association, epithelial sensing that is indeed enhanced by microinvasion. This occurs both by epithelial endocytosis and paracellular migration resulting in epithelial innate responses that are not entirely pneumolysin dependent and that is associated with bacterial clearance. These data implicate epithelial microinvasion in the initiation of bacterial clearance which to the benefit of the colonising pathogen may also enhance transmission.

Methods

Bacteria

S. pneumoniae clinical strains used were 6B (BHN 418[35]), 23F (P1121[36]) and TIGR4 (P1672[37]), together with a pneumolysin deficient TIGR4 mutant strain (kind gift from Prof T Mitchell, University of Birmingham). Stocks of bacterial aliquots grown to O.D 0.3 were stored at -80ºC, defrosted, resuspended in cell culture media and used once. Colony forming units were counted on horse blood agar plates (EO Labs).

Experimental Human Pneumococcal Carriage Model (EHPC)

Following written informed consent, healthy non-smoking adults between the ages of 18 – 59 were inoculated with 80,000 CFU live 6B *S. pneumoniae* (BHN418), grown to mid-log phase in vegetone broth as previously described[38]. All volunteers were negative for the pneumococcus at baseline. Nasal washes and mucosal cells (curette biopsy) from the inferior turbinate were obtained by PBS syringe and curettage using a plastic Rhino-probe™ (Arlington Scientific, Springville, UT), respectively before pneumococcal inoculation. These were then repeated on days 2, 6, 9, 14 - 27 post inoculation[39]. Bacteria collected from nasal washes were quantified by CFU counts. Two curettage samples were obtained and processed for confocal immunofluorescence, flow cytometry, primary cell culture and /or transcriptomic analysis by RNAseq.

Ethical approval was given by NHS Research and Ethics Committee (REC)/Liverpool School of Tropical Medicine (LSTM) REC, reference numbers: 15/NW/0146 and 14/NW/1460 and Human Tissue Authority licensing number 12548.

169 **Human Respiratory Tract Epithelial Cells**

170 Human pharyngeal carcinoma Detroit 562 epithelial cells (ATCC_CCL-138) and human
171 bronchial carcinoma Calu3 epithelial cells (ATCC_HTB-55) were grown in 10% FCS in alpha
172 MEM media (Gibco). Human alveolar epithelial carcinoma A549 epithelial cells
173 (ATCC_CCL-185) were grown in 10% FCS with 1% L-glutamine in Hams/F-12 media
174 (Gibco).

175

176 **Pneumococcal-epithelial cell co-culture**

177 *Association and Invasion assays* - confluent Detroit 562 (day 8 post plating), Calu3 (day 10
178 post plating) and A549 (day 4 post plating) monolayers were cultured on 12 well plates
179 (Corning) were exposed to *S. pneumoniae* for three hours in 1% FCS alpha MEM. The
180 medium was removed and cells washed three times in $HBSS^{+/+}$. Cells were incubated in 1%
181 saponin for 10 minutes at 37°C and lysed by repetitive pipetting. Dilutions of bacteria were
182 plated on blood agar and colonies counted after 16 hours. To quantify internalised bacteria,
183 100µg/ml gentamicin was added for 1 hour to the cells, which were then washed another
184 three times, before incubating with Saponin and plating on blood agar plates. Colony forming
185 units (CFU) were counted after 16 hours incubation at 37°C, 5% CO_2. There were no
186 differences in pneumococcal pre- or post-inoculum, or density between the strains, in the
187 cell supernatant three hours post-infection.
188 *Transmigration assay* - Detroit 562 cells were cultured on 3µm pore, PET Transwell Inserts
189 (ThermoFisher) for 10 days to achieve confluent, polarised monolayers. Calu3 cells were
190 plated onto Transwell inserts for 12 days and A549 cells for 6 days. Cell culture media was
191 changed 1 hour prior to addition of bacteria to 1% FCS (250µl apical chamber, 1ml basal
192 chamber). Resistance was recorded before and after *S. pneumoniae* were added using an
193 EVOM2 (World Precision Instruments). 1mg/ml FITC-dextran (Sigma Aldrich) was added to
194 the apical chamber of selected inserts to assess permeability. Approximately 12 million (±

195 5.7 x 10^6) bacteria were added to the cells (~MOI 1 cell : 25 bacteria). During the time course,
196 50µl was removed, diluted and plated, from the basal chamber to measure bacterial load by
197 counting CFU/well. Permeability was recorded using a FLUOstar Omega (BMG Labtech) at
198 488nm.
199 *Inhibition assays* - Detroit 562 cells cultured on 12 well plates were treated with 80µM
200 Dynasore (Cambridge Biosciences) and 7.5µg/ml Nystatin (Sigma Aldrich) to block
201 endocytosis; or 1µM Cytochalasin D (Bio Techne Ltd) to block actin polymerisation, for 30
202 minutes prior to, and for the duration of pneumococcal infection incubation period. DMSO
203 was used as a control. Cells were washed and treated with gentamicin and lysed in saponin
204 as described above.
205
206 **Confocal Microscopy**
207 For the *in vivo* analysis, mucosal cells derived by curettage from the EHPC model were
208 placed directly into 4% PFA for 1 hour. Cells were cytospun onto microscope slides and
209 allowed to air dry. For the *in vitro* analysis, epithelial cell lines on transwell membranes were
210 fixed in either 4% PFA (Pierce, Methanol Free) or 1:1 mix of methanol:acetone for 20
211 minutes. Cells were permeabilised with 0.2% Triton X-100 for 10 minutes and blocked for 1
212 hour in blocking buffer (3% goat serum and 3% BSA in PBS) before incubation with anti-6B
213 pneumococcal antisera, JAM-A, Claudin 4 or β catenin primary antibodies (see
214 Supplementary Information) for one hour and then secondary and/or conjugated antibodies
215 for 45 minutes. DAPI solution was added for 5 minutes. After washing, the stained samples
216 were mounted using Aqua PolyMount (VWR International) with a coverslip onto a microslide.
217 The entire cytospin for each sample was manually viewed by microscopy for detection of
218 pneumococci. Multiple fields of view were imaged for each transwell insert, for each
219 condition. Images were captured using either an inverted LSM 700, LSM 880, or

TissueFAXS Zeiss Confocal Microscope. Z stacks were recorded at 1µm intervals at either 40x oil or 63x oil objectives.

Flow cytometry

For the *in vivo* analysis, two nasal scrapes were used per sample. Cells on rhinoprobes incubated in cold PBS++ (PBS supplemented with 5mM EDTA and 0.5% FCS) were dislodged by pipetting and centrifuged at 440g for 5 mins at 4^{o}C. Supernatant was removed and cells resuspended in 25ul of PBS with Live/Dead^{TM} Fixable Violet Dead Cell Stain (ThermoFisher). After 15 minutes incubation on ice, antibody cocktail (see Supplementary Information) was added and incubated for another 15 minutes. 500µl of PBS++ was added to a 70µm filter before vortexing the samples and adding 3.5mls of PBS and filtering over the wet filter. Samples were transferred to a 5ml FACS tube, centrifuged and resuspended in 200µl Cell Fix (BD Biosciences). Samples were acquired on LSRII Flow Cytometer (BD Biosciences). Analyses of data was performed on the gated epithelial cell population and only samples containing 500 or more cells were considered for interpretation.

For the *in vitro* analysis, confluent monolayers of Detroit 562 cells on 6 well plates were incubated with *S. pneumoniae* for 6 hours in 1% FCS phenol free alpha MEM (base media, Life Technologies). Cells were washed three times in PBS and gently lifted from the plate using a cell scraper in 300µl of base media supplemented with 1mM EDTA. Samples were transferred to 5ml FACS tubes and placed on ice for the duration of the protocol. Each cell sample was incubated with an antibody cocktail (see supplemental information) were added to the cells for 30 minutes before rinsing in 1ml base media and centrifuging at 300g for 5 minutes at 4^{o}C. Cells were fixed in 600µl of 4% PFA and run through LSR II Flow Cytometer (BD Biosciences). Compensation was run and applied for each experimental replicate and voltages consistent throughout. Isotype controls (BD Biosciences), FL-1 and single stains

were also run for each experiment. Samples were acquired until 300,000 events had been collected. Analyses was performed using FlowJo version 10 software.

ELISAs

Supernatent from Detroit 562 cells that had been incubated with *S. pneumoniae* for 6 hours, was collected for cytokine analysis. IL-1beta, IL-6, IL-8, IFNg, TNFa, ICAM-1 DuoSet® ELISA kits were purchased from R&D Systems and protocol followed according to manufacturers' instructions.

RNA samples and sequencing (RNASeq)

Mucosal curettage samples and epithelial cell cultures (incubated with or without *S. pneumoniae* for 3 hours) were collected in RNALater (ThermoFisher) at -80C until extraction. Extraction was performed using the RNEasy micro kit (Qiagen) with on column DNA digestion. RNA was treated for DNA using Turbo DNA-free Kit (Qiagen) and cleaned using RNEasy Micro kit (Qiagen). Extracted RNA quality was assessed and quantified using a BioAnalyser (Agilent 2100). Library preparation and RNA-sequencing (Illumina Hiseq4000, 20M reads, 100 paired-end reads) were performed at the Beijing Genome Institute (China) or the Sanger Institute for mucosal curettage samples. *In vitro* samples used the KAPA Stranded mRNA-Seq Kit (Roche Diagnostics) to construct stranded mRNA-seq libraries from 500 ng intact total RNA after which paired-end sequencing was carried out using a 75-cycle high-output kit on the NextSeq 500 desktop sequencer (Illumina Platform, performed by the PGU, UCL).

Paired end reads were mapped to the Ensembl human transcriptome reference sequence (homo sapiens GRCh38, latest version). Mapping and generation of read counts per transcript were performed using Kallisto[40], based on pseudoalignment. R/Bioconductor

package tximport was used to import the mapped counts data and summarise the transcripts-level data into gene level[41]. Further analyses were run using DESeq2 and the SARTools packages[42]. Normalisation and differential analyses were run using DESeq2 by use of a negative binomial generalised linear model. The estimates of dispersion and logarithmic fold changes incorporate data-driven prior distributions. SARTools, which is an R pipeline based on DESeq2, was used to generate lists of differentially expressed genes and diagnostic plots for quality control. Using these techniques, cells exposed to different *S. pneumoniae* strains were compared against non-infected control cells, and extracted a result table with log2fold changes, Wald test p values and adjusted p values (according to false discovery rate, FDR).

Pathways and networks analyses were performed using XGR R package[43]. For each strain genes that were upregulated compared to the non-infected samples with an adjusted p-value (FDR) < 0.05 were selected. Network analyses were performed using as nodes the upregulated genes labelled with significance (FDR). Four gene subnetworks were generated using the Pathway Common database which contains directed interactions from a physical and pathways aspect. These new lists were then used for enrichment analysis (hypergeometric test) to identify enriched pathways from the REACTOME database. Enriched pathways were then represented in a heat map using log2 z-scores. REACTOME database has a non-structured list of terms, therefore terms were clustered based on overlapping genes. All heat maps were produced with a heat map R package using Euclidean distances and hierarchical clustering. The same gene lists were used to test for enrichment in Gene Ontology cellular components and membrane-related terms were selected. Upstream regulator analysis was performed in Ingenuity Pathway Analysis (IPA). Venn diagrams were generated using http://bioinformatics.psb.ugent.be/webtools/Venn/.

297 *In vivo* data were processed with the same pipeline used for the *in vitro* experiments. Mapped reads
298 ranged between 16M to 66M. Upregulated gene lists were produced and only genes with a log2
299 FC>1 were used for further pathway analysis. Pathway analysis with REACTOME database was
300 performed with InnateDB. TPM for all genes were obtained and transformed into log2 scale. Quality
301 control for 75 samples showed a batch effect due to two different labs sequencing the data. Combat
302 function in the SVA R package was used[44] to reduce this effect. Principal component analysis
303 identified an outlier that was removed for further analysis. Using the gene interactome lists for each
304 strain from the *in vitro* data, a pan signature or module was obtained which included 200 genes that
305 were upregulated in at least one strain. 16 genes were shared among all strains. Module scores for
306 each group were derived by calculating the log2 average gene expression for each module. A non-
307 parametric (Mann-Whitney) test was performed to compare carriers to non-carriers for each time
308 point. Violin plots were produced with in house script in R and ggplot2[43].
309
310 **Statistics**
311 All experiments were conducted with replicates in three or more independent experiments
312 unless stated otherwise. Error bars represent SEM unless stated otherwise. GraphPad
313 Prism Version 10 was used to perform parametric (t-tests or ANOVA) or non-parametric
314 (Mann-Whitney or Kruskal-Wallis tests) analysis, which was based on the Shapiro-Wilk
315 normality test. P values lower than 0.05 were considered significant.
316
317 **RESULTS**
318 ***Streptococcus pneumoniae* colonisation of the human nasal mucosal is associated**
319 **with adhesion, microcolony formation and microinvasion**
320 We have used an Experimental Human Pneumococcal Carriage Model[45] to characterise
321 pneumococcal-epithelial interactions *in vivo*. Colonisation was detected in 9/13 healthy
322 volunteers by culture, 11/13 by microscopy and 9/11 by LytA PCR (Table 1). The carriage
323 status of each volunteer in the study was blinded until sample collection was completed.

Differences in the results obtained with each detection method may reflect methodological threshold detection, or the location and therefore the accessibility of the colonising pneumococci (e.g. in the mucus escalator vs. adherence to the epithelial cell surface). Nonetheless, all three methods demonstrated that colonisation was established and that clearance largely occurred between day 9 and 27 (Table 1 and Figure 1B).

Curette biopsy samples yielded intact sheets of epithelial cell associated with immune cells visualised by confocal microscopy (Figure 1A and Supplementary Figure 1A). Pneumococcal surface adhesion increased over time and was associated with microcolony formation (Figure 1E, middle and right panels). This provides evidence that the EHPC model represents true carriage and colonisation of the pneumococci. There was also evidence of pneumococcal microinvasion through the epithelial monolayer (Figure 1C and 1D) which comprised both endocytosis (Figure 1E left and middle panels) and paracellular migration (Figure 1E, left panel). Internalised pneumococci were also observed in immune cells (Supplementary Figure 1A).

Co-association between pneumococci and the junctional protein JAM-A was also observed (Figure 1F). JAM-A is a tight junction protein which is important for the regulation of barrier function in the respiratory epithelium[46]. These bacteria were either located at junctions between cells (left panel) or internalised inside cells (right panel). Junctional association of *S. pneumoniae* were also observed with nasal epithelial cells grown in culture *ex-vivo*, differentiated on an air-liquid interface for 30 days and then co-cultured with either 6B or 23F *S. pneumoniae* (Supplementary Figure 1B). Microcolony formation and internal pneumococci were also observed in these cell cultures.

Epithelial surface marker expression in response to *Streptococcus pneumoniae in vivo*

We stained the nasal curette biopsies for surface expression of IL-22Ra1, HLADR, CD40, CD54 or CD107a. Epithelial cells were identified by EpCAM expression (Supplementary Figure 2A-D for Flow Cytometry parameters). IL-22Ra1 is expressed exclusively on epithelial cells[47] and is considered to protect the epithelial barrier and promote anti-microbial product secretion during infection, in response to IL-22 secretion by immune cells[48,49]. In the context of pneumococcal infection in mice, IL-22 appears to play an important role in carriage and clearance[50,51]. In the EHPC model, there was a trend towards increased expression of IL-22Ra1 at day 9, (when clearance starts to occur) in the carriage positive, compared to the carriage negative volunteers, although this did not reach statistical significance (Figure 2A, 2B top). We did not detect any change in the relative expression of inflammatory marker HLADR[52] on the nasal epithelium in carriers vs. non-carriers over time (Figure 2A, 2B, second row). Similarly, epithelial surface expression of CD40, a costimulatory protein which binds CD154 (CD40L) and CD54 (Intercellular Adhesion Molecule 1, ICAM-1) a key leukocyte adhesion molecule which is also upregulated by CD40[53-55], and plays a role in neutrophil migration and recruitment[56-59], did not change over time. Finally, we assessed the expression of CD107a, also known as lysosomal associated membrane protein 1 (LAMP-1) which is a marker for natural killer cell activity[60] and in the epithelium, forms the membrane glycoprotein of lysosomes and endosomes[27]. CD107a has been shown to be cleaved during infection with *Neisseria* species which are also extracellular mucosal pathogens[61]. Although the number of epithelial cells expressing CD107a did not change over time (Figure 2A, bottom), we did observe an increase intensity of expression at day 2 post inoculation in carriage positive volunteers vs. carriage negative volunteers, which was maintained throughout the remainder of the time course.

Epithelial adherence, endocytosis and transmigration by *Streptococcus pneumoniae* varies by pneumococcal strain and is modulated by pneumolysin

To further investigate our observations from the EPHC, we undertook epithelial co-culture experiments with the cell line Detroit 562, derived from a nasal pharyngeal carcinoma. We used the EHPC 6B strain and two other representative clinical isolates serotype 4 (TIGR4, the original sequences strain) and 23F. Any differences between these strains are not simply explained by differential growth during colonisation (data not shown). Although they may be partially explained by capsule serotype[37,62], TIGR4, 23F and 6B genome comparisons have revealed ~15,000 single nucleotide polymorphisms and insertion/deletion mutations (SNPs and INDELS) not related to capsule (data not shown). We have also used a TIGR4 strain where pneumolysin, a key virulence factor that is associated with pore-forming induced inflammation[15,23] has been knocked out (kind gift from Prof. TJ Mitchell, University of Birmingham, UK).

Strikingly, the number of TIGR4 pneumococci associated with the Detroit 562 cells was ten-fold higher than 6B or 23F strains (Figure 3A). This pattern was also observed by immunofluorescence (Figure 3D and 3E, and Supplementary Figure 4). Epithelial adhesion was associated with internalisation within the cells (Figure 3B) into what appeared to be intracellular vesicles that were coated in host proteins, in this case JAM-A (Figure 3G and Figure 5A), which indicates vesicular endocytosis and using bacteria that are pre-stained with FAMSE, we were able to distinguish extracellular bacteria (blue) from those below the apical surface prior to permeabilization of the cells (green, Figure 3F). Interestingly, co-association with another tight junction protein, Claudin 4, was not readily observed, while occasional co-association with the adherens junction protein β catenin was observed (Supplementary Figure 4A and 4B).

To assess transmigration, pneumococci that had penetrated the basal chamber of cells cultured on transwell inserts were counted. Although only statistically significant at 1hr between 23F and TIGR4, 23F was more readily detected compared to the other strains (Figure 3C). By microscopy, we observed laterally located bacteria, and pneumococci zip-wiring between cell junctions (Figure 3H). We observed pneumococci at the level of the nuclei and below the basal membrane (Figure 3I). This was more readily, but not exclusively, seen with the 23F strain. These data demonstrate a similar pattern of interaction between the *S. pneumoniae* 6B strain and human epithelium *in vivo* and *in vitro*; and show that the relative prominence of adhesion, endocytosis and paracellular transmigration varies by genotype.

Pneumolysin deletion in the TIGR4 mutant showed a significant increase in internalisation (Figure 3B) and an increase in transmigration capacity (Figure 3C). These data suggest that interactions within epithelial cells are in part, regulated by pneumolysin.

Loss of epithelial cell barrier function is not a pre-requisite for microinvasion by *S. pneumoniae*

Several mucosal pathogens including *S. pneumoniae*, are known to directly, and indirectly affect the integrity of epithelial barriers and tight junction function[25,27,28,61,63-67]. It was not possible to directly assess epithelial barrier function during colonisation in the EHPC model. We have therefore explored the possibility that over the same time frame where we have observed pneumococcal adhesion and microinvasion, epithelial surface molecule upregulation and cytokine production *in vitro*, there is epithelial barrier function disruption. Trans-epithelial electrical resistance (TEER) is not high in Detroit 562 cells but nevertheless TEER was not affected by pneumococcal co-culture (Figure 3J). To assess permeability,

4kDa FITC-dextran was applied to the apical chamber of transwells and epithelial leak quantified from the basal chamber. With the Detroit 562 cells, a significant reduction in permeability was seen with 6B pneumococci, 23F and TIGR4 (23 – 34%), compared to non-infected cells (Figure 3K). This implicates a role for pneumolysin in epithelial integrity.. These data suggest that loss of epithelial cell barrier function is not a pre-requisite for pneumococcal adhesion and microinvasion, and that as described in murine models[23,25], changes to barrier function appear pneumolysin dependent.

To explore the possibility that our findings were not cell line dependent, we also used A549 cells (Supplementary Figure 3A-E), which are undifferentiated alveolar Type II pneumocytes, and Calu3 cells (Supplementary Figure 3F-J), which represent a more polarised and differentiated cell originally derived from bronchial submucosa. Pneumococcal behaviour with both cell lines was similar, although absolute intensity of adhesion, microinvasion and transmigration differed (Supplementary Figure 3A and 3F, Supplementary Figure 3B and 3G, and Supplementary Figure 3C and 3H, respectively). This may in part be due to the high expression of polymeric Immunoglobulin Receptor found on Detroit cells[63], and differential barrier function with A549 cells having the least trans-epithelial electrical resistance and the most permeability (Supplementary Figure 3D and 3E, respectively), and Calu3 having the greatest trans-epithelial electrical resistance and the least permeability (Supplementary Figure 3I and 3J, respectively). Importantly, no change in barrier function was seen with these cells. As with Detroit 562 cells, for A549 and Calu3 cells TEER (Supplementary Figure DA and 3I) and permeability (Supplementary Figure 3E and 3J) was preserved following exposure to pneumococci for three hours. Indeed, if anything, epithelial co-culture resulted in an enhanced barrier function as shown via an increase in TEER (Supplementary Figure 3D) and a decrease in permeability to TIGR4 (Supplementary Figure 3E) in A549 cells.

Streptococcus pneumoniae **upregulates epithelial surface CD54 and CD107a** ***in vitro***

It is uncertain whether the observed, at best, modest surface changes seen in the 6B EHPC model reflect a relatively silent host response to colonization by this strain, or was confounded by inter-volunteer variation. We have therefore compared the impact of the pneumococcal strains on Detroit 562 cell expression of the same range of surface markers. (See Supplementary Figure 2E-G for Flow Cytometry parameters). There was no significant change in epithelial markers IL-22Ra1, HLADR or CD40 (Figure 4A and 4B). However, although not seen with the 6B or 23F strains, $CD54^{high}$ expression was significantly greater for TIGR4 and dPLY strains, compared to non-infected cells. Epithelial CD107a, which has previously been implicated in pneumococcal endocytosis[27] was upregulated in response to the 6B, 23F and TIGR4 strains (Figure 4A and 4B, bottom graphs), but was not seen with the pneumolysin TIGR4 mutant. These data again demonstrate a similar pattern of interaction between the *S. pneumoniae* 6B strain and human epithelium *in vivo* and *in vitro, implicating* pneumolysin in the induction of CD54 but not CD107a surface expression.

S. pneumoniae **upregulates epithelial inflammatory cytokines and soluble CD54** ***in vitro***

To further investigate the inflammatory potential of the epithelium, measured for IL-6, IL-8 and CD54 secretion in the supernatants of Detroit 562 cells following incubation with pneumococci (Figure 4C). We have detected a significant increase in IL-6 and IL-8 ($P = <0.0001$), which was not entirely pneumolysin dependent. In line with the surface marker observations, only TIGR4 significantly upregulated the secretion of soluble CD54 ($P = 0.0013$), which was dependent on the presence of pneumolysin (Figure 4C). Other cytokine responses to *S. pneumoniae,* such as IFNγ, IL-1β and TNFα were below the limits of detection (Data not shown).

476 **Internalised pneumococci do not replicate within the epithelium**

477 *S. pneumoniae* is generally considered to be an extracellular bacterium[68]. However, since
478 we and others have observed intracellular bacteria[27], we wanted to test whether they remain
479 viable, can replicate, and egress from the epithelial cell. Pneumococci that adhere on the
480 epithelial cell surface are capable of replicating, as demonstrated by epithelial surface
481 microcolony formation in the 6B EHPC model (Figure 1E). In contrast, the pneumococci that
482 were identified by confocal microscopy to be intracellular, were often single bacterial cells,
483 co-localised with host proteins (Figure 5A) and did not appear to increase in number over
484 time (Figure 5B). Bacteria that had transmigrated across the epithelial monolayer *in vitro* did
485 replicate and remained viable for at least three hours post removal of the transwell insert
486 (Figure 5C). To test the hypothesis that intracellular migration is not permissive for bacterial
487 growth, we co-cultured pneumococci with epithelial cells for three hours, treated with
488 gentamicin for one hour, replenished the media and recorded CFUs over time from the
489 apical and basal chamber of transwell inserts (Figure 5D and E, respectively). Although
490 bacteria were detected at low levels, replication was not readily apparent. To test whether
491 these bacteria transmigrated across the cells in a transcellular or paracellular manner, we
492 inhibited endocytosis by cellular treatment with Dynasore and Nystatin, or actin
493 polymerisation by cellular treatment with Cytochalasin D. We found that the inhibition of
494 endocytosis prevented transmigration but the inhibition of actin polymerisation enhanced
495 transmigration in Detroit 562 cells with 23F pneumococci (data not shown).

496

497 ***Streptococcus pneumoniae* induces epithelial innate transcriptomic responses that**
498 **is influenced by the pattern of epithelial adhesion and microinvasion**

499 To further explore the hypothesis that the pattern of epithelial adhesion and microinvasion
500 results in differential epithelial sensing and therefore epithelial inflammatory-response

genes, we performed RNAseq and obtained transcriptomic data from our pneumococci infected Detroit 562 cells. As shown in Figure 6A, we found that TIGR4 upregulated 1127 genes (550 unique genes), 23F upregulated 650 genes (69 unique genes), and 6B upregulated only 153 genes (10 unique genes) compared to non-infected cells. The pneumolysin mutant upregulated 220 genes (14 unique genes). 93 genes were upregulated by all strains compared to non-infected cells. These findings appeared to reflect the invasive and inflammatory nature of these bacteria in this *in vitro* epithelial model. To further explore the nature of these differences, we performed pathway analyses using the REACTOME database and performed with XGR(Figure 6B). Again, we found that the upregulated pathways for TIGR4 and 23F were pro-inflammatory, but that the 6B profile was relatively silent. For example, TIGR4 upregulated pathways involved innate immunity, such as TLR signalling, cytokine signalling and stress responses. In comparison, 6B increased pathways involved in NOD and NRL signalling, and gene regulation. The TIGR4 pneumolysin mutant transcriptomic profile suggested that pneumolysin modulates epithelial cell RIG-I/MDA5 mediated induction of IFN-α/β activation of IRF and NFκB pathways. In line with the cytokine profiles that we observed at the protein level, we detected upregulation of IL-6, IRAK2, TNFAIP3 and CD54 genes (Figure 6C) within the innate immune pathways selected (Supplementary Figure 5A). In line with our previous observation, 6B elicited the least and TIGR4 the greatest transcriptomic response. Given the pneumococcus interacts with the epithelial cell surface, analysis of genes associated with host cell membrane components were analysed at the transcriptomic level (Figure 6D) using Gene Ontology database (Cellular component terms only, Supplementary Figure 5B). Analysis of genes associated with host cell membrane components showed that the tight junction protein Claudin 4 was upregulated in response to 23F and TIGR4. Claudin 4 is normally associated with a tight barrier in epithelial cells[69,70], which would support our hypothesis that the epithelium responds to preserve barrier function during co-culture.

Further bioinformatics analysis of upstream regulators revealed that RELA, or the nuclear factor NFκB p65 subunit is likely to be a key mediator of these pneumococcal-epithelial interactions (Figure 6E, Supplementary Figure 5C). Comparisons between the strains again reveal a more silent upstream profile with 6B compared to TIGR4 or 23F.

Epithelial transcriptomic responses to *S. pneumoniae in vivo* are most marked around the time of bacterial clearance

To test whether the relatively silent transcriptomic profile seen with the *S. pneumoniae* 6B strain during *in vitro* co-culture, was also present *in vivo,* we have first had to design an approach to focus on the epithelial response in the curette biopsy tissue. Using the *in vitro* epithelial transcriptomic data, we have derived an integrated transcriptome signature that allows us to interrogate the epithelial RNAseq transcriptomic response obtained from the 6B EHPC model (Supplementary Figure 6A). Within the cohort (Supplementary Figure 6B), the number of significantly upregulated genes was low (Figure 7A). However, looking at the genes average of the epithelial signatures' genes (200 genes for the Integrated and 16 genes for the Core signature), we observed a shift in gene expression following 6B inoculation that was maximal at day 9, coinciding with the time of maximal bacterial clearance (Figure 7B, and Figure 7C, Integrated and Core signatures). Qualitatively, there was a shift from generic homeostasis at baseline towards a metabolic and innate defence profile at day 2, and surface receptor upregulation and inflammatory signalling pathways by day 9 (Figure 7A).

DISCUSSION

The upper respiratory tract is at the centre of the control of colonisation by a wide range of commensal bacteria. For some more pathogenic members of this commensal community, epithelial sensing and the triggering of inflammation may result in bacterial clearance but may also promote onward transmission. By combining *in vitro* cell culture systems and the EHPC model, we have shown that human epithelial sensing of the pneumococcus is enhanced by microinvasion, resulting in an epithelial inflammatory/innate immune response that is temporally associated with clearance.

We have demonstrated that the pneumococcus interacts with the human respiratory epithelium and that the innate epithelial cell response is dependent on the association of the bacteria (Figure 8). We show that colonisation leads to adherence, microcolony formation and microinvasion within the epithelium, which results in activation of signalling pathways that lead to cytokine and chemokine upregulation, biochemical and metabolic pathway enrichment. However, although microinvasion does not support bacterial growth, co-association with junctional proteins provides a possible mechanism for migration across the barrier, that could ultimately affect transmission or cause invasive disease. We provide evidence of epithelial sensing of the pneumococcus that coincides with clearance in the EHPC model.

The occurrence of microinvasion during colonisation in healthy individuals is supported by murine colonisation experiments[71] and the detection of pneumococcal DNA in the blood of healthy colonised children[72]. Using primary and immortalised epithelial cell line models that mirror this process, and in line with other cell culture and murine models[64,66,71,73], we have demonstrated that pneumococcal microinvasion occurs by endocytosis and the formation of

cytoplasmic vacuoles, and by paracellular transcytosis. Transcriptomic analysis of the epithelial response *in vitro* and *in vivo* has revealed that the pattern of pneumococcal epithelial surface adherence and microinvasion determines the host cell response through a range of innate signalling and regulatory pathways, inflammatory mediators, adhesion molecules, cellular metabolism and stress response genes. These data support the view that beyond forming a physical barrier, secreting mucus, and modulating the transport of immunoglobulins, the epithelium plays a critical role in the regulation of these complex host-pathogen interactions[19,74,75].

Nasal colonisation in murine models is proinflammatory[24,76] and is associated with epithelial microinvasion and tight junction modulation[25]. Our *in vitro* epithelial model co-culture with a serotype 6B strain suggests that this is not always the case with only modest pneumococcal-host cell adherence, endocytosis and paracellular migration, and a relatively silent epithelial inflammatory profile. Indeed, volunteers who undergo EHPC generally remain clinically asymptomatic and this silent transcriptomic pattern of epithelial response is mirrored in the 6B EHPC model, where we have observed surface adherence, microcolony formation and some microinvasion.

After three hours infection *in vitro*, we did not observe a breakdown of epithelial barrier function. Previous studies in mice and human lung tissue that have investigated infection over longer periods of incubation, have seen tight junction dysregulation[25,64], and we did observe co-association with junctional proteins such as JAM-A and β catenin. IN accordance with studies in human alveolar cells[64], Claudin 4 was not affected by the pneumococcus, although we did detect a transcriptomic upregulation in Detroit cells. In mice, changes in claudin regulation was TLR dependent [25,77] and we detected TLR4 and TLR3 activation in

our Detroit 562 cells transcriptomic analyses, in response to all strains of the pneumococci we tested. Previous studies have implicated pneumolysin to activate TLR2 and TLR4 stimulated cytokine release, such as IL-6 and IL-8, both of which we detected in infected Detroit 562 cell supernatants[30,78]. Interestingly, TLR3 is normally associated with double stranded RNA detection of viruses, such as Influenza[79]. There appears to be a relationship between the outcome of infection between Influenza and *S. pneumoniae*[79,80], which may be important for understanding the dynamics of flu vaccination success. TLR3 leads to the activation of IRF3 and the secretion of type 1 interferons[81,82]. Type 1 interferons have been shown to be stimulated in response to murine pneumococcal infection that leads to bacterial clearance[83,84]. Here, the authors also show anti-microbial product secretion, and we detected evidence of β defensin gene upregulation in the EHPC model two days post inoculation with 6B (Figure 7A). We also detected upregulation of RIG-I/MDA5 mediated induction of IFN-α/β pathways following *in vitro* stimulation with the TIGR4 pneumolysin mutant, providing further evidence that sensing by the epithelium may be important. DNA sensing of *S. pneumoniae* has been demonstrated in alveolar macrophages, where secretion of Type 1 Interferons led to upregulation of STING and the transcription factor IFN regulatory factor 3, augmented by pneumolysin[76,84].

Pneumolysin, a pore forming toxin, has been implicated as a major virulence factor contributing to host inflammation and transmission[23,85]. We found pneumolysin to be a prominent trigger of epithelial surface molecule upregulation, cytokine production and the transcriptomic inflammatory response *in vitro*. The prominence of TLR4 signalling pathways in the transcriptomic profile observed and the presence of TLR4 on epithelial cells, implicates pneumolysin. Mediated by autolysin, the pneumococcus undergoes autolysis when reaching stationery growth phase, resulting in the release of additional PAMPs including bacterial DNA. We therefore suggest that in the context of microinvasion,

627 pneumococcal DNA may act as an alternative epithelial sensing agonist to induce
628 inflammation. Furthermore, cellular entry of DNA may be enhanced by pneumolysin pore
629 formation[84]. In mice, pneumococcal DNA triggers inflammation through a
630 DAI/STING/TBK1/IRF3 cascade[76,84], a response that contributes to pneumococcal
631 clearance. Indeed, we observed an increased epithelial expression of the lysosomal
632 membrane protein CD107a, following pneumococcal co-infection.

633

634 Our findings are limited by the number of pneumococcal strains that can be safely tested in
635 an EHPC model to enable direct comparisons between the *in vivo* and *in vitro* data.
636 Nonetheless, the use of different strains *in vitro* has enabled us and others[73,86] to interrogate
637 the impact of different patterns of epithelial adherence and invasion on the host
638 inflammatory/ innate immune response. Transcriptomic analysis has enabled us to postulate
639 the potential epithelial sensing pathways but these will need to be fully defined in more
640 precise model systems. We have placed considerable reliance on the findings from
641 immortalised cell lines from relevant tissue but our findings have been reassuringly
642 paralleled by our findings in primary cell lines derived from the EHPC and the EHPC itself.

643

644 Our data highlight the complex interactions between the host epithelium and *S. pneumoniae*
645 whereby pneumococcal microinvasion may ultimately dictate the outcome of colonisation,
646 altering the delicate balance between inflammation-mediated transmission and clearance
647 (Figure 8). Ultimately, epithelial sensing of pneumococcal-epithelial interaction and its
648 outcome may be dictated by the bacterial strain, the force of infection, or the frequency of
649 co-colonisation of pneumococcal strains, (more important in children and high carriage
650 prevalence populations), viral co-infections and other environmental pressures[1,20,87].
651 Measures of human to human transmission are needed to fully understand the critical

pathways and a mechanistic insight into the impact of pneumococcal vaccine on epithelial adhesion and invasion is required if we are to improve herd protection.

Acknowledgements

This study was funded by the Wellcome Trust (Grant 106846/Z/15/Z). DF is supported by the Medical Research Council (grant MR/M011569/1), Bill and Melinda Gates Foundation (grant OPP1117728) and the National Institute for Health Research (NIHR) Local Comprehensive Research Network. LytA PCR was performed by Prof. D Bogaert, University of Edinburgh, UK. RNAseq library preparation undertaken at UCL was provided by the Pathogens Genomic Unit. Confocal imaging facilities at LSTM were funded by a Wellcome Trust Multi-User Equipment Grant (104936/Z/14/Z). Flow cytometric acquisition was funded by a Wellcome Trust Multi-User Equipment Grant (104936/Z/14/Z).

Author contributions: CMW, SPJ, DMF and RSH conceived and designed the study. CMW, SP, SPJ, JR, EN, CS, CA acquired the data. CMW, CV, SPJ, MN, JSB, DMF, RSH analysed and interpreted the data. CMW wrote the first draft of the manuscript. CMW, CV, SP, SPJ, JR, EN, CS, CA, MN, JSB, DMF, RSH commented on and approved the manuscript.

Conflicts of interest: the authors declare no conflicts of interest.

REFERENCES

1. O'Brien, K.L., *et al.* Burden of disease caused by Streptococcus pneumoniae in children younger than 5 years: global estimates. *Lancet* **374**, 893-902 (2009).

2. Kagnoff, M.F. The intestinal epithelium is an integral component of a communications network. *J Clin Invest* **124**, 2841-2843 (2014).

3. Jochems, S.P., Weiser, J.N., Malley, R. & Ferreira, D.M. The immunological mechanisms that control pneumococcal carriage. *PLoS Pathog* **13**, e1006665 (2017).

4. Shiri, T., *et al.* Indirect effects of childhood pneumococcal conjugate vaccination on invasive pneumococcal disease: a systematic review and meta-analysis. *Lancet Glob Health* **5**, e51-e59 (2017).

5. Whitney, C.G., *et al.* Decline in invasive pneumococcal disease after the introduction of protein-polysaccharide conjugate vaccine. *N Engl J Med* **348**, 1737-1746 (2003).

6. Usuf, E., Bottomley, C., Adegbola, R.A. & Hall, A. Pneumococcal carriage in sub-Saharan Africa--a systematic review. *PLoS One* **9**, e85001 (2014).

7. Brueggemann, A.B., Pai, R., Crook, D.W. & Beall, B. Vaccine escape recombinants emerge after pneumococcal vaccination in the United States. *PLoS Pathog* **3**, e168 (2007).

8. Hanage, W.P., *et al.* Carried pneumococci in Massachusetts children: the contribution of clonal expansion and serotype switching. *Pediatr Infect Dis J* **30**, 302-308 (2011).

9. Pillai, D.R., *et al.* Genome-wide dissection of globally emergent multi-drug resistant serotype 19A Streptococcus pneumoniae. *BMC Genomics* **10**, 642 (2009).

10. Mosser, J.F., *et al.* Nasopharyngeal carriage and transmission of Streptococcus pneumoniae in American Indian households after a decade of pneumococcal conjugate vaccine use. *PLoS One* **9**, e79578 (2014).

11. Pido-Lopez, J., Kwok, W.W., Mitchell, T.J., Heyderman, R.S. & Williams, N.A. Acquisition of pneumococci specific effector and regulatory Cd4+ T cells localising within human upper respiratory-tract mucosal lymphoid tissue. *PLoS Pathog* **7**, e1002396 (2011).

12. Glennie, S.J., *et al.* Regulation of Naturally Acquired Mucosal Immunity to Streptococcus pneumoniae in Healthy Malawian Adults and Children. *PLoS One* **7**, e51425 (2012).

13. Zhang, Q., *et al.* Characterisation of regulatory T cells in nasal associated lymphoid tissue in children: relationships with pneumococcal colonization. *PLoS Pathog* **7**, e1002175 (2011).

14. Lipsitch, M., *et al.* Are Anticapsular Antibodies the Primary Mechanism of Protection against Invasive Pneumococcal Disease? *PLoS Med* **2**, e15 (2005).

15. Ratner, A.J., *et al.* Epithelial cells are sensitive detectors of bacterial pore-forming toxins. *J Biol Chem* **281**, 12994-12998 (2006).

16. Ratner, A.J., Lysenko, E.S., Paul, M.N. & Weiser, J.N. Synergistic proinflammatory responses induced by polymicrobial colonization of epithelial surfaces. *Proc Natl Acad Sci U S A* **102**, 3429-3434 (2005).

17. Eisele, N.A. & Anderson, D.M. Host Defense and the Airway Epithelium: Frontline Responses That Protect against Bacterial Invasion and Pneumonia. *J Pathog* **2011**, 249802 (2011).

18. Ganesan, S., Comstock, A.T. & Sajjan, U.S. Barrier function of airway tract epithelium. *Tissue Barriers* **1**, e24997 (2013).

19. Whitsett, J.A. & Alenghat, T. Respiratory epithelial cells orchestrate pulmonary innate immunity. *Nat Immunol* **16**, 27-35 (2015).

20. Plotkowski, M.C., Puchelle, E., Beck, G., Jacquot, J. & Hannoun, C. Adherence of type I Streptococcus pneumoniae to tracheal epithelium of mice infected with influenza A/PR8 virus. *Am Rev Respir Dis* **134**, 1040-1044 (1986).

21. Pittet, L.A., Hall-Stoodley, L., Rutkowski, M.R. & Harmsen, A.G. Influenza virus infection decreases tracheal mucociliary velocity and clearance of Streptococcus pneumoniae. *Am J Respir Cell Mol Biol* **42**, 450-460 (2010).

22. McCullers, J.A., Iverson, A.R., McKeon, R. & Murray, P.J. The platelet activating factor receptor is not required for exacerbation of bacterial pneumonia following influenza. *Scand J Infect Dis* **40**, 11-17 (2008).

23. Zafar, M.A., Wang, Y., Hamaguchi, S. & Weiser, J.N. Host-to-Host Transmission of Streptococcus pneumoniae Is Driven by Its Inflammatory Toxin, Pneumolysin. *Cell Host Microbe* **21**, 73-83 (2017).

24. Wilson, R.*, et al.* Protection against Streptococcus pneumoniae lung infection after nasopharyngeal colonization requires both humoral and cellular immune responses. *Mucosal Immunol* **8**, 627-639 (2015).

25. Clarke, T.B., Francella, N., Huegel, A. & Weiser, J.N. Invasive bacterial pathogens exploit TLR-mediated downregulation of tight junction components to facilitate translocation across the epithelium. *Cell Host Microbe* **9**, 404-414 (2011).

26. Agarwal, V., Asmat, T.M., Dierdorf, N.I., Hauck, C.R. & Hammerschmidt, S. Polymeric immunoglobulin receptor-mediated invasion of Streptococcus pneumoniae into host cells requires a coordinate signaling of SRC family of protein-tyrosine kinases, ERK, and c-Jun N-terminal kinase. *J Biol Chem* **285**, 35615-35623 (2010).

27. Asmat, T.M., Agarwal, V., Saleh, M. & Hammerschmidt, S. Endocytosis of Streptococcus pneumoniae via the polymeric immunoglobulin receptor of epithelial cells relies on clathrin and caveolin dependent mechanisms. *Int J Med Microbiol* **304**, 1233-1246 (2014).

28. Beisswenger, C., Coyne, C.B., Shchepetov, M. & Weiser, J.N. Role of p38 MAP kinase and transforming growth factor-beta signaling in transepithelial migration of invasive bacterial pathogens. *J Biol Chem* **282**, 28700-28708 (2007).

29. Ratner, A.J., Aguilar, J.L., Shchepetov, M., Lysenko, E.S. & Weiser, J.N. Nod1 mediates cytoplasmic sensing of combinations of extracellular bacteria. *Cell Microbiol* **9**, 1343-1351 (2007).

30. Malley, R.*, et al.* Recognition of pneumolysin by Toll-like receptor 4 confers resistance to pneumococcal infection. *Proc Natl Acad Sci U S A* **100**, 1966-1971 (2003).

31. Gewirtz, A.T., Navas, T.A., Lyons, S., Godowski, P.J. & Madara, J.L. Cutting edge: bacterial flagellin activates basolaterally expressed TLR5 to induce epithelial proinflammatory gene expression. *J Immunol* **167**, 1882-1885 (2001).

32. Gewirtz, A.T.*, et al.* Salmonella typhimurium translocates flagellin across intestinal epithelia, inducing a proinflammatory response. *J Clin Invest* **107**, 99-109 (2001).

33. Hornef, M.W., Wick, M.J., Rhen, M. & Normark, S. Bacterial strategies for overcoming host innate and adaptive immune responses. *Nat Immunol* **3**, 1033-1040 (2002).

34. Ferreira, D.M.*, et al.* Controlled human infection and rechallenge with Streptococcus pneumoniae reveals the protective efficacy of carriage in healthy adults. *Am J Respir Crit Care Med* **187**, 855-864 (2013).

35. Browall, S.*, et al.* Intraclonal variations among Streptococcus pneumoniae isolates influence the likelihood of invasive disease in children. *J Infect Dis* **209**, 377-388 (2014).

36. McCool, T.L., Cate, T.R., Moy, G. & Weiser, J.N. The immune response to pneumococcal proteins during experimental human carriage. *J Exp Med* **195**, 359-365 (2002).

37. Hyams, C., Camberlein, E., Cohen, J.M., Bax, K. & Brown, J.S. The Streptococcus pneumoniae capsule inhibits complement activity and neutrophil phagocytosis by multiple mechanisms. *Infect Immun* **78**, 704-715 (2010).

38. Collins, A.M.*, et al.* First human challenge testing of a pneumococcal vaccine. Double-blind randomized controlled trial. *Am J Respir Crit Care Med* **192**, 853-858 (2015).

39. Jochems, S.P.*, et al.* Novel Analysis of Immune Cells from Nasal Microbiopsy Demonstrates Reliable, Reproducible Data for Immune Populations, and Superior Cytokine Detection Compared to Nasal Wash. *PLoS One* **12**, e0169805 (2017).

40. Bray, N.L., Pimentel, H., Melsted, P. & Pachter, L. Near-optimal probabilistic RNA-seq quantification. *Nat Biotechnol* **34**, 525-527 (2016).

41. Soneson, C., Love, M.I. & Robinson, M.D. Differential analyses for RNA-seq: transcript-level estimates improve gene-level inferences. *F1000Res* **4**, 1521 (2015).

42. Varet, H., Brillet-Gueguen, L., Coppee, J.Y. & Dillies, M.A. SARTools: A DESeq2- and EdgeR-Based R Pipeline for Comprehensive Differential Analysis of RNA-Seq Data. *PLoS One* **11**, e0157022 (2016).

43. Fang, H., Knezevic, B., Burnham, K.L. & Knight, J.C. XGR software for enhanced interpretation of genomic summary data, illustrated by application to immunological traits. *Genome Med* **8**, 129 (2016).

44. Chakraborty, S., Datta, S. & Datta, S. Surrogate variable analysis using partial least squares (SVA-PLS) in gene expression studies. *Bioinformatics* **28**, 799-806 (2012).

785 45. Wright, A.K., *et al.* Human nasal challenge with Streptococcus pneumoniae is immunising in the
786 absence of carriage. *PLoS Pathog* **8**, e1002622 (2012).
787 46. Mitchell, L.A., *et al.* Junctional adhesion molecule A promotes epithelial tight junction assembly
788 to augment lung barrier function. *Am J Pathol* **185**, 372-386 (2015).
789 47. Wolk, K., *et al.* IL-22 increases the innate immunity of tissues. *Immunity* **21**, 241-254 (2004).
790 48. Pham, T.A., *et al.* Epithelial IL-22RA1-mediated fucosylation promotes intestinal colonization
791 resistance to an opportunistic pathogen. *Cell Host Microbe* **16**, 504-516 (2014).
792 49. Zheng, M., *et al.* Therapeutic Role of Interleukin 22 in Experimental Intra-abdominal Klebsiella
793 pneumoniae Infection in Mice. *Infect Immun* **84**, 782-789 (2016).
794 50. Van Maele, L., *et al.* Activation of Type 3 innate lymphoid cells and interleukin 22 secretion in
795 the lungs during Streptococcus pneumoniae infection. *J Infect Dis* **210**, 493-503 (2014).
796 51. Trevejo-Nunez, G., Elsegeiny, W., Conboy, P., Chen, K. & Kolls, J.K. Critical Role of IL-22/IL22-
797 RA1 Signaling in Pneumococcal Pneumonia. *J Immunol* **197**, 1877-1883 (2016).
798 52. Fais, S., *et al.* HLA-DR antigens on colonic epithelial cells in inflammatory bowel disease: I.
799 Relation to the state of activation of lamina propria lymphocytes and to the epithelial expression of
800 other surface markers. *Clin Exp Immunol* **68**, 605-612 (1987).
801 53. Propst, S.M., Denson, R., Rothstein, E., Estell, K. & Schwiebert, L.M. Proinflammatory and Th2-
802 derived cytokines modulate CD40-mediated expression of inflammatory mediators in airway
803 epithelia: implications for the role of epithelial CD40 in airway inflammation. *J Immunol* **165**, 2214-
804 2221 (2000).
805 54. Dugger, K., Lowder, T.W., Tucker, T.A. & Schwiebert, L.M. Epithelial cells as immune effector
806 cells: the role of CD40. *Semin Immunol* **21**, 289-292 (2009).
807 55. Cagnoni, F., *et al.* CD40 on adult human airway epithelial cells: expression and proinflammatory
808 effects. *J Immunol* **172**, 3205-3214 (2004).
809 56. Huang, G.T., Eckmann, L., Savidge, T.C. & Kagnoff, M.F. Infection of human intestinal epithelial
810 cells with invasive bacteria upregulates apical intercellular adhesion molecule-1 (ICAM)-1)
811 expression and neutrophil adhesion. *J Clin Invest* **98**, 572-583 (1996).
812 57. Bianco, A., *et al.* Expression of intercellular adhesion molecule-1 (ICAM-1) in nasal epithelial
813 cells of atopic subjects: a mechanism for increased rhinovirus infection? *Clin Exp Immunol* **121**, 339-
814 345 (2000).
815 58. Sumagin, R., *et al.* Neutrophil interactions with epithelial-expressed ICAM-1 enhances intestinal
816 mucosal wound healing. *Mucosal Immunol* **9**, 1151-1162 (2016).
817 59. Frick, A.G., *et al.* Haemophilus influenzae stimulates ICAM-1 expression on respiratory epithelial
818 cells. *J Immunol* **164**, 4185-4196 (2000).
819 60. Alter, G., Malenfant, J.M. & Altfeld, M. CD107a as a functional marker for the identification of
820 natural killer cell activity. *J Immunol Methods* **294**, 15-22 (2004).
821 61. Lin, L., *et al.* The Neisseria type 2 IgA1 protease cleaves LAMP1 and promotes survival of
822 bacteria within epithelial cells. *Mol Microbiol* **24**, 1083-1094 (1997).

62. Aprianto, R., Slager, J., Holsappel, S. & Veening, J.W. Time-resolved dual RNA-seq reveals extensive rewiring of lung epithelial and pneumococcal transcriptomes during early infection. *Genome Biol* **17**, 198 (2016).

63. Zhang, J.R.*, et al.* The polymeric immunoglobulin receptor translocates pneumococci across human nasopharyngeal epithelial cells. *Cell* **102**, 827-837 (2000).

64. Peter, A.*, et al.* Localization and pneumococcal alteration of junction proteins in the human alveolar-capillary compartment. *Histochem Cell Biol* **147**, 707-719 (2017).

65. Coyne, C.B. The distinct roles of JAM-A in reovirus pathogenesis. *Cell Host Microbe* **5**, 3-5 (2009).

66. Short, K.R.*, et al.* Influenza virus damages the alveolar barrier by disrupting epithelial cell tight junctions. *Eur Respir J* **47**, 954-966 (2016).

67. Weight, C.M., Jones, E.J., Horn, N., Wellner, N. & Carding, S.R. Elucidating pathways of Toxoplasma gondii invasion in the gastrointestinal tract: involvement of the tight junction protein occludin. *Microbes Infect* **17**, 698-709 (2015).

68. Henriques-Normark, B. & Tuomanen, E.I. The pneumococcus: epidemiology, microbiology, and pathogenesis. *Cold Spring Harb Perspect Med* **3**(2013).

69. Mitchell, L.A., Overgaard, C.E., Ward, C., Margulies, S.S. & Koval, M. Differential effects of claudin-3 and claudin-4 on alveolar epithelial barrier function. *Am J Physiol Lung Cell Mol Physiol* **301**, L40-49 (2011).

70. Rokkam, D., Lafemina, M.J., Lee, J.W., Matthay, M.A. & Frank, J.A. Claudin-4 levels are associated with intact alveolar fluid clearance in human lungs. *Am J Pathol* **179**, 1081-1087 (2011).

71. Mahdi, L.K., Ogunniyi, A.D., LeMessurier, K.S. & Paton, J.C. Pneumococcal virulence gene expression and host cytokine profiles during pathogenesis of invasive disease. *Infect Immun* **76**, 646-657 (2008).

72. Morpeth, S.C.*, et al.* Detection of Pneumococcal DNA in Blood by Polymerase Chain Reaction for Diagnosing Pneumococcal Pneumonia in Young Children From Low- and Middle-Income Countries. *Clin Infect Dis* **64**, S347-S356 (2017).

73. Bootsma, H.J., Egmont-Petersen, M. & Hermans, P.W. Analysis of the in vitro transcriptional response of human pharyngeal epithelial cells to adherent Streptococcus pneumoniae: evidence for a distinct response to encapsulated strains. *Infect Immun* **75**, 5489-5499 (2007).

74. Zanin, M., Baviskar, P., Webster, R. & Webby, R. The Interaction between Respiratory Pathogens and Mucus. *Cell Host Microbe* **19**, 159-168 (2016).

75. Vareille, M., Kieninger, E., Edwards, M.R. & Regamey, N. The airway epithelium: soldier in the fight against respiratory viruses. *Clin Microbiol Rev* **24**, 210-229 (2011).

76. Koppe, U.*, et al.* Streptococcus pneumoniae stimulates a STING- and IFN regulatory factor 3-dependent type I IFN production in macrophages, which regulates RANTES production in macrophages, cocultured alveolar epithelial cells, and mouse lungs. *J Immunol* **188**, 811-817 (2012).

77. Beisswenger, C., Lysenko, E.S. & Weiser, J.N. Early bacterial colonization induces toll-like receptor-dependent transforming growth factor beta signaling in the epithelium. *Infect Immun* **77**, 2212-2220 (2009).

78. Schmeck, B.*, et al.* Pneumococci induced TLR- and Rac1-dependent NF-kappaB-recruitment to the IL-8 promoter in lung epithelial cells. *Am J Physiol Lung Cell Mol Physiol* **290**, L730-L737 (2006).

79. Spelmink, L.*, et al.* Toll-Like Receptor 3/TRIF-Dependent IL-12p70 Secretion Mediated by Streptococcus pneumoniae RNA and Its Priming by Influenza A Virus Coinfection in Human Dendritic Cells. *MBio* **7**, e00168-00116 (2016).

80. Rudd, J.M., Ashar, H.K., Chow, V.T. & Teluguakula, N. Lethal Synergism between Influenza and Streptococcus pneumoniae. *J Infect Pulm Dis* **2**(2016).

81. Chen, N.*, et al.* RNA sensors of the innate immune system and their detection of pathogens. *IUBMB Life* **69**, 297-304 (2017).

82. Alexopoulou, L., Holt, A.C., Medzhitov, R. & Flavell, R.A. Recognition of double-stranded RNA and activation of NF-kappaB by Toll-like receptor 3. *Nature* **413**, 732-738 (2001).

83. Joyce, E.A., Popper, S.J. & Falkow, S. Streptococcus pneumoniae nasopharyngeal colonization induces type I interferons and interferon-induced gene expression. *BMC Genomics* **10**, 404 (2009).

84. Parker, D.*, et al.* Streptococcus pneumoniae DNA initiates type I interferon signaling in the respiratory tract. *MBio* **2**, e00016-00011 (2011).

85. Hotomi, M., Yuasa, J., Briles, D.E. & Yamanaka, N. Pneumolysin plays a key role at the initial step of establishing pneumococcal nasal colonization. *Folia Microbiol (Praha)* **61**, 375-383 (2016).

86. Novick, S.*, et al.* Adhesion and invasion of Streptococcus pneumoniae to primary and secondary respiratory epithelial cells. *Mol Med Rep* **15**, 65-74 (2017).

87. Glennie, S.J., Williams, N.A. & Heyderman, R.S. Mucosal immunity in resource-limited setting: is the battle ground different? *Trends Microbiol* **18**, 487-493 (2010).

FIGURE LEGENDS

Table 1. *Streptococcus pneumoniae* association with the nasal epithelium in the EHPC model detected by culture, confocal microscopy and LytA PCR

Nasal washes and nasal curette biopsies were collected from carriage positive and carriage negative volunteers over time. Standard methods for measuring bacterial density by culture (CFU) and LytA PCR were compared against counts visualised by confocal microscopy for pneumococcal association with nasal cells over time. The data was derived from 13 volunteers. + (1-10 pneumococci); ++ (11-50 pneumococci); +++ (51-100 pneumococci); ++++ (>100 pneumococci) ND = not done.

Figure 1. *Streptococcus pneumoniae* colonisation of the human nasal epithelium is associated with adhesion, microcolony formation and microinvasion

(A) Nasal curette biopsies were processed from the EHPC model. Images show representative fields demonstrating that areas of intact epithelium can be obtained from the samples (as visualised by XY planes) and they retain their size and shape (as visualised by XZ planes). Cells were stained with Wheat Germ Agglutinin (WGA) or JAM-A (red) and nuclei (blue). (B) Graphical representation of the pattern of pneumococcal density detected by culture and microscopy. (C) The proportion of bacteria located on the cell surface, intracellularly, or paracellularly visualized by confocal microscopy, quantified from 8 volunteers collected over time. Data is derived from microscopy counts. The cells were stained for surface carbohydrates using WGA, and the bacteria were marked with specific serotype antiserum. (D) XY images of 1µm slices through a layer of cells, with bacteria associated. XY image of cells showing (Ei) bacterial internalization, (Eii) and microcolony formation on the surface of an epithelial cell, with one intracellular bacterium. (Eiii) XZ and YZ stacks demonstrating surface association of single and multiple bacteria per cell (top),

916 possible migration through the epithelium either internally or between cells (middle), and
917 residing at or below the level of the cell nuclei (bottom). (F) Co-association between *S.*
918 *pneumoniae* (green) and JAM-A (red). Nuclei (blue). Internalised bacteria were also
919 observed to be co-associated with JAM-A.

920

921 **Figure 2. Epithelial surface marker expression in response to *Streptococcus***
922 ***pneumoniae in vivo* analysed by flow cytometry**

923 (A) Median fluorescence intensity for IL-22Ra, HLADR, CD40, CD54 or CD107a. (B) High
924 surface marker-expressing cells (>95% of the baseline expression). Results are from a
925 minimum of two volunteers. Black squares are carriage negative and grey circles are
926 carriage positive. There were no significant differences in surface marker expression
927 between the carriage positive and negative samples.

928

929 **Figure 3. Epithelial adherence, endocytosis and transmigration by *Streptococcus***
930 ***pneumoniae,* the influence of pneumolysin and the impact on barrier function**

931 Detroit 562 cell monolayers (approximately $1x10^6$ per well) were stimulated with $7x10^6$
932 pneumococci ± $2.75x10^6$ for 3 hours and the quantity of bacteria (A) associated with the
933 cells, and (B) internalized inside the cells, were determined by culture (CFU). N = >6
934 independent experiments with replicates. **** P = <0.0001. (C) Detroit 562 cells cultured on
935 transwell inserts were stimulated with approximately $1.2x10^7$ pneumococci ± $6x10^6$ for 3
936 hours and the quantity of bacteria in the basal chamber was determined over time. P values
937 at 0.5hr = 0.1751; 1hr, * P = 0.0187; 2hr, P = 0.1222; 3hr, P = 0.0740. N = 5 independent
938 experiments with replicates. (D) Representative pneumococcal-density images of Detroit
939 562 cells following three hours infection. (E-I) Representative images illustrating differences
940 in association between strains on epithelial cells stained with JAM-A. (E) Difference in

surface density of pneumococci between 6B and TIGR4; (F) apical association of bacteria (extracellular blue) and green (below the level of the apical surface,), co-association with JAM-A; (G) internalisation of bacteria as shown in JAM-A associated intracellular vesicle-like bodies; (H) lateral localisation of the pneumococci (top) with possible paracellular movement across the monolayer (bottom); (I) basal localisation of bacteria both at the nuclei level and the transwell insert pore level. Images are representative of examples across all experiments (n = >20) and across Detroit 562 cells, Calu3 cells and A549 cells.

Detroit 562 cells were exposed with pneumococci for three hours on transwell inserts and TEER and permeability were recorded. (K) The average TEER for these cells was 19Ω.cm^2 (±15Ω.cm^2, data not shown). ANOVA shows a significant effect from calcium withdrawal *** P = 0.0013 (n = 3). There was no difference in TEER between non-infected and pneumococcal-infected cells, P = 0.6334. n = 9 independent experiments with replicates. (J) Permeability was assessed by leak to 4kDa FITC-dextran. N = >4 independent experiments. **** P = <0.0001 comparing non-infected against pneumococcal strains.

Figure 4. Modulation of epithelial surface molecule expression, cytokine and soluble CD54 secretion by *Streptococcus pneumoniae in vitro*

(A) Monolayers of Detroit 562 cells were stimulated with *S. pneumoniae* for 6 hours and the median fluorescence intensity for each epithelial activation marker was analysed by flow cytometry. (B) High-expressing cells for each marker were compared against non-infected cells, which were set at 5%. n = >3 independent experiments. * P < 0.05 CD54; **** P < 0.0001 CD107a median and *** P < 0.001 CD107a 5%, all comparing non-infected to strains of pneumococci (except median CD107a, TIGR4 v dPLY where P = 0.0009 and 5% CD107a, TIGR4 v dPLY where P = 0.0286). (C) IL-6, IL-8 and CD54 in the supernatants from Detroit

562 cells stimulated with *S. pneumoniae* for 6 hours were measured by ELISA. Results represent six independent experiments with replicates. **** P <0.0001 IL-6; *** P = 0.0013 CD54; **** P < 0.0001 IL-8).

Figure 5. Pneumococci internalised within the epithelium do not replicate

(A) Representative images of internalised pneumococci co-localised with JAM-A as indicated by the arrows (B) A549 cells were incubated with *S. pneumoniae* for three hours, washed, treated with gentamicin for 1 hour, and the cultures were incubated for further time points to measure bacterial internalisation (B). Data represents three independent experiments with replicates. **** P = <0.0001. (C) Detroit 562 cells were incubated with pneumococci for three hours on transwell inserts which were then removed and bacteria in the basal chamber were further incubated in the absence of cells. (n = 5 for three hours, n = 2 for 4 hours, n = 1 for 5 hours (latter error bars S.D)). (D and E) Detroit 562 cells were incubated with *S.pneumoniae* for three hours, washed, treated with gentamicin for one hour, washed, and bacteria that were released into the apical (D) or basal (E) chamber were counted. N = 3 independent experiments with replicates. Similar results were also observed with Calu 3 cells (data not shown).

Figure 6. *Streptococcus pneumoniae* induces epithelial innate transcriptomic responses *in vitro* that are influenced by the pattern of epithelial adhesion and microinvasion

(A) The total number of epithelial genes upregulated following exposure to 6B, 23F, TIGR4 and TIGR4-dPLY pneumococci, compared to non-infected samples. Genes with an FDR <0.05 were considered for further analysis. The matrix shows intersections for the four

strains, sorted by size. Dark circles in the matrix indicates sets that are part of the intersection. (B) Clustered heat map representing the log2 zeta scores of REACTOME Pathway Analysis of epithelial cells exposed to pneumococci. For clarity, only pathways with a p-value of 0.001 are represented. Clustered heat maps representing the log2 fold-changes for genes of pathways involved in (C) innate immunity and (D) membrane components. Genes that are not upregulated (I.E. where the FDR is above 0.05 and not in the interactome) are coloured in light grey. (E) Using the upstream regulator analysis in IPA, transcription regulators with an activated Z-score greater than 2, were compared following exposure to each strain of pneumococci. The 20-most activated epithelial transcription regulators are shown in the table.

Figure 7. Epithelial transcriptomic responses to *Streptococcus pneumoniae* in the EHPC model are most marked around the time of bacterial clearance

(A) The overlap of upregulated genes between time points and significant REACTOME pathways. (B) Log2 TPM arithmetic mean for genes in the integrated interactome module. (C) Log2 TPM arithmetic mean for genes in the core interactome module. RNA from nasal curette biopsies was used to identify genes that were upregulated with a log2 fold-change of ≥1 were compared between baseline (day minus 4) and 2 and 9 days post inoculation of 6B in the EHPC model. Epithelial modules were generated from the *in vitro* epithelial RNA data.

Figure 8. Model of the control of pneumococcal colonisation by the human mucosal epithelium.

Following pneumococcal adhesion and microcolony formation on the epithelial surface, the host response is dependent on the subsequent pattern of interaction. Microinvasion (endocytosis and paracellular transmigration) amplifies epithelial sensing and inflammation/ innate immunity, which we postulate leads to immune cell engagement. This process of epithelial sensing inflammation/ innate immunity may enhance both transmission and clearance. Co-association with junctional proteins may facilitate migration across the barrier.

Table 1

	Microbiology density (CFU/ml)					Microscopy counts					LytA PCR					Association		
Vol	**Pre**	**D2**	**D6**	**D9**	**D27**	**Pre**	**D2**	**D6**	**D9**	**D27**	**Pre**	**Day 2**	**Day 6**	**Day 9**	**Day 27**	**Surface**	**Intracellular**	**Lateral**
1	0	370	520	10	1.6	0	+	+	0	+	NEG	POS	POS	ND	POS	+	0	0
2	0	0	0	0	0	0	+	0	0	0	NEG	NEG	NEG	ND	NEG	++	+	0
3	0	0	0	0	0	0	+	+	0	0	NEG	POS	NEG	ND	NEG	+	0	0
4	0	2.8	8.8	0	0	0	0	0	+	0	NEG	POS	POS	ND	NEG	+	0	0
5	0	$7x10^3$	220	21	0	0	+	+	+	0	ND	ND	ND	ND	ND	+	+	0
6	0	$1.9x10^4$	$5.7x10^3$	$3.7x10^4$	11	0	++	++++	++	0	NEG	POS	POS	ND	POS	+++	++	+
7	0	820	$1.1x10^3$	160	0	0	+	+++	++	0	NEG	POS	POS	ND	NEG	++	+	+
8	0	0	0	0	0	0	0	0	0	+	ND	ND	ND	ND	ND	0	0	0
9	0	220	700	3.8	0.04	ND	+	+++	+	ND	NEG	POS	POS	ND	NEG	+++	+	+
10	0	$1x10^3$	0.04	0.04	0	ND	0	+	0	ND	NEG	POS	POS	ND	POS	+	0	0
11	0	$1.8x10^6$	$1.8x10^6$	$1.9x10^4$	0.08	ND	+++	++++	+	ND	NEG	POS	POS	ND	NEG	+++	+	+
12	0	0	0	0	0	ND	++	0	0	ND	NEG	NEG	NEG	ND	NEG	++	+	+
13	0	23	1.7	0	0	ND	+	0	0	ND	POS	POS	POS	ND	POS	+	0	0

Figure 1

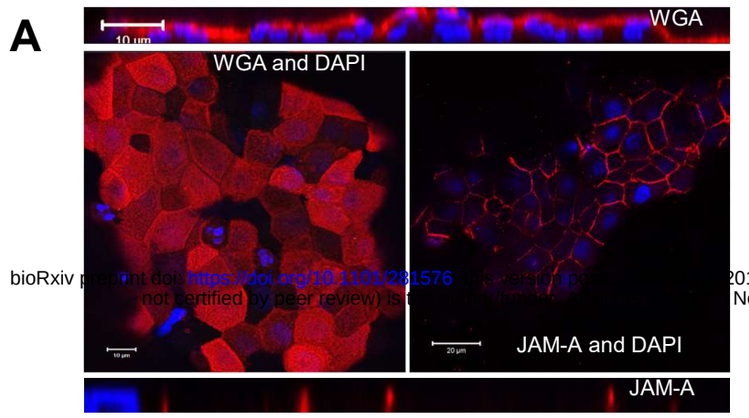

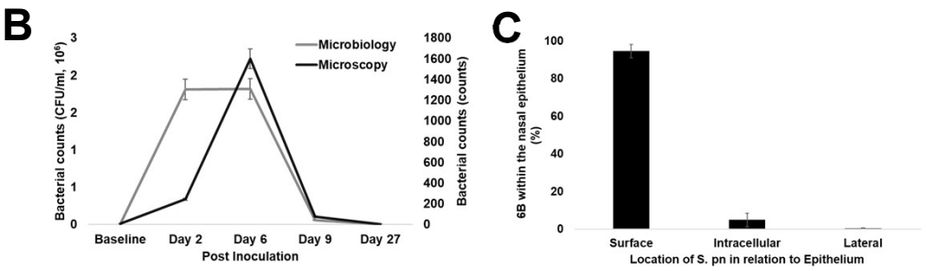

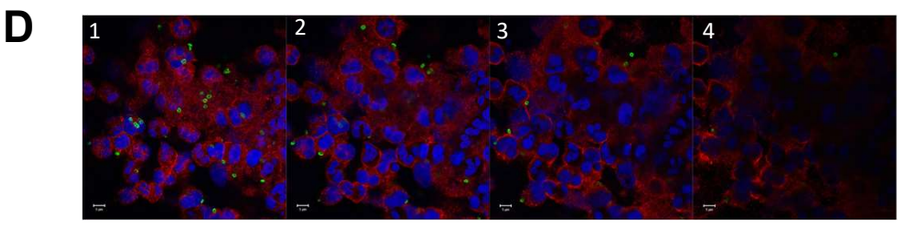

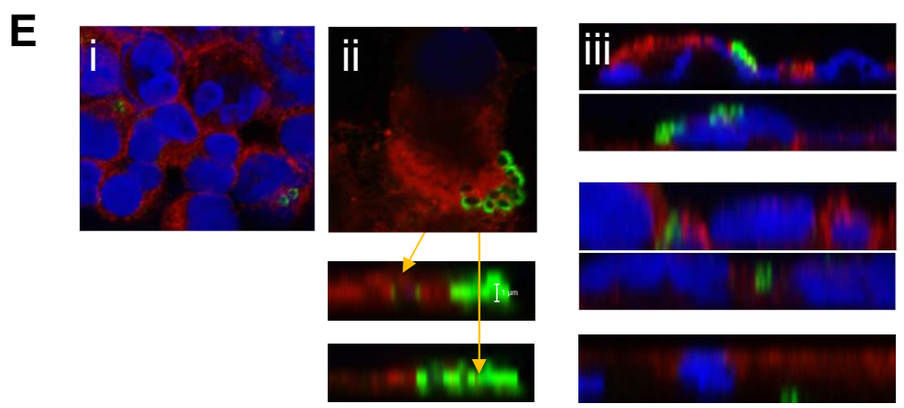

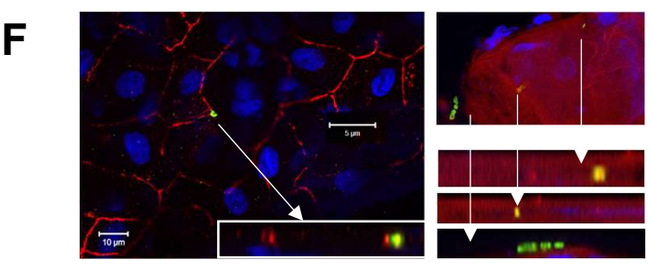

Figure 2

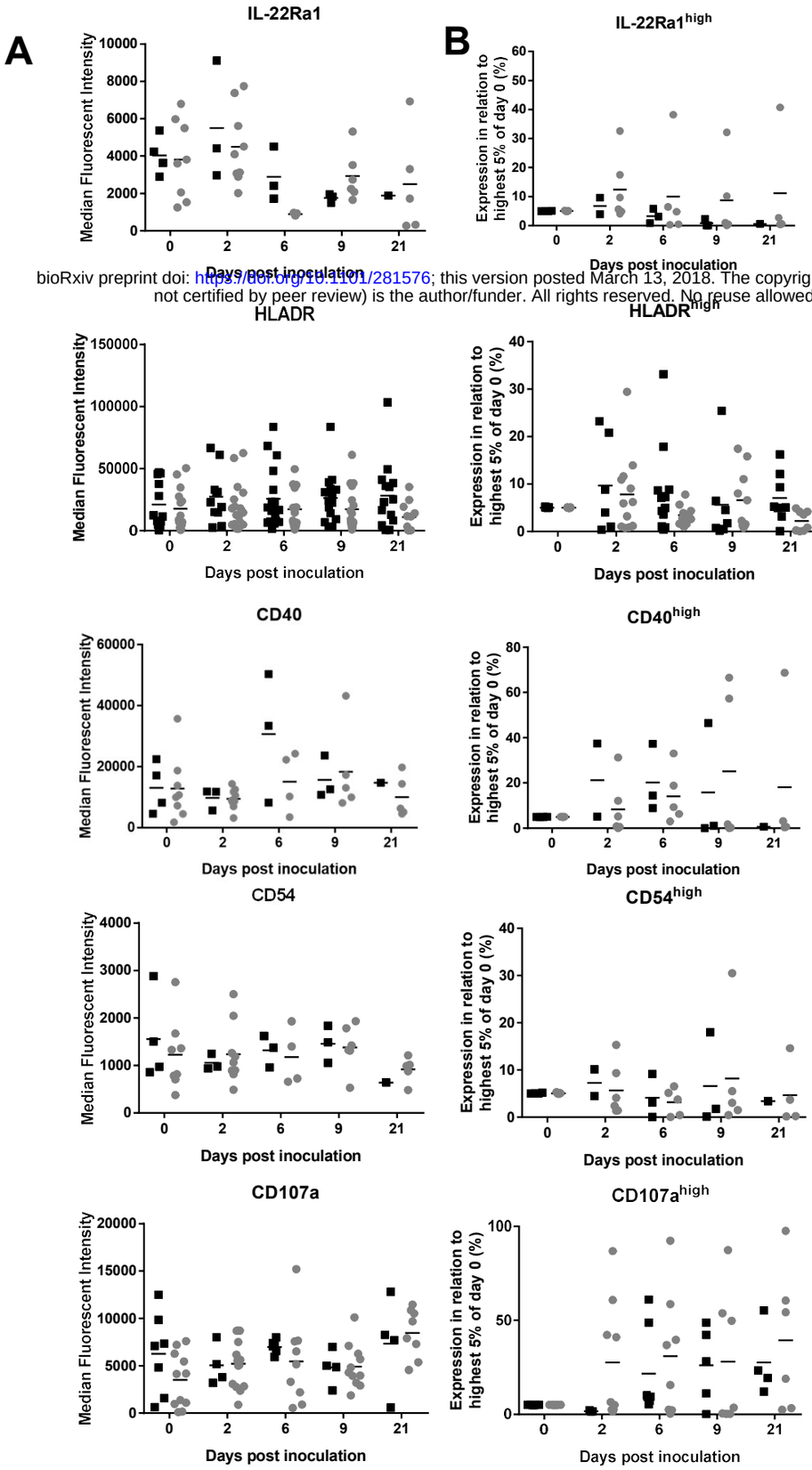

Figure 3

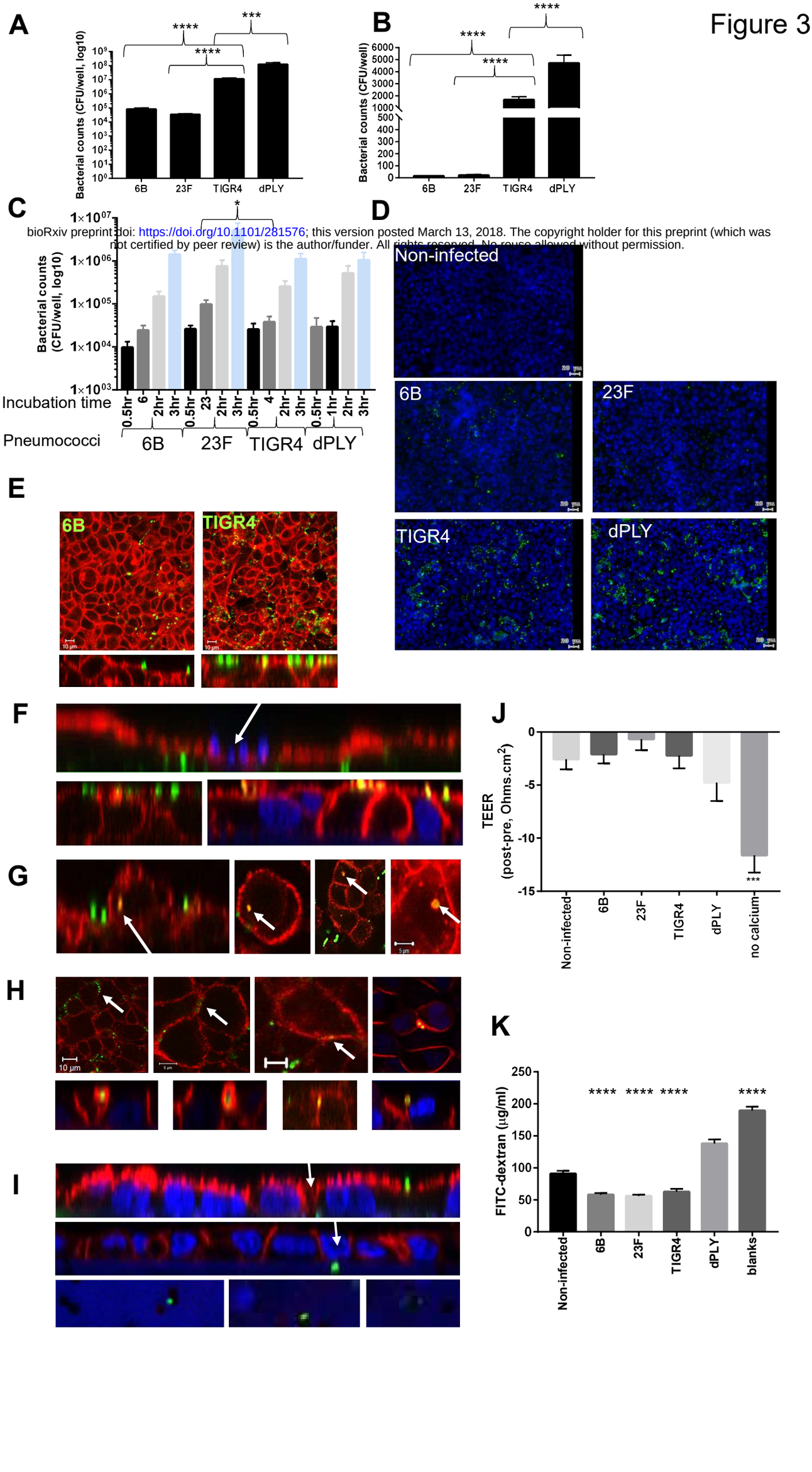

Figure 4

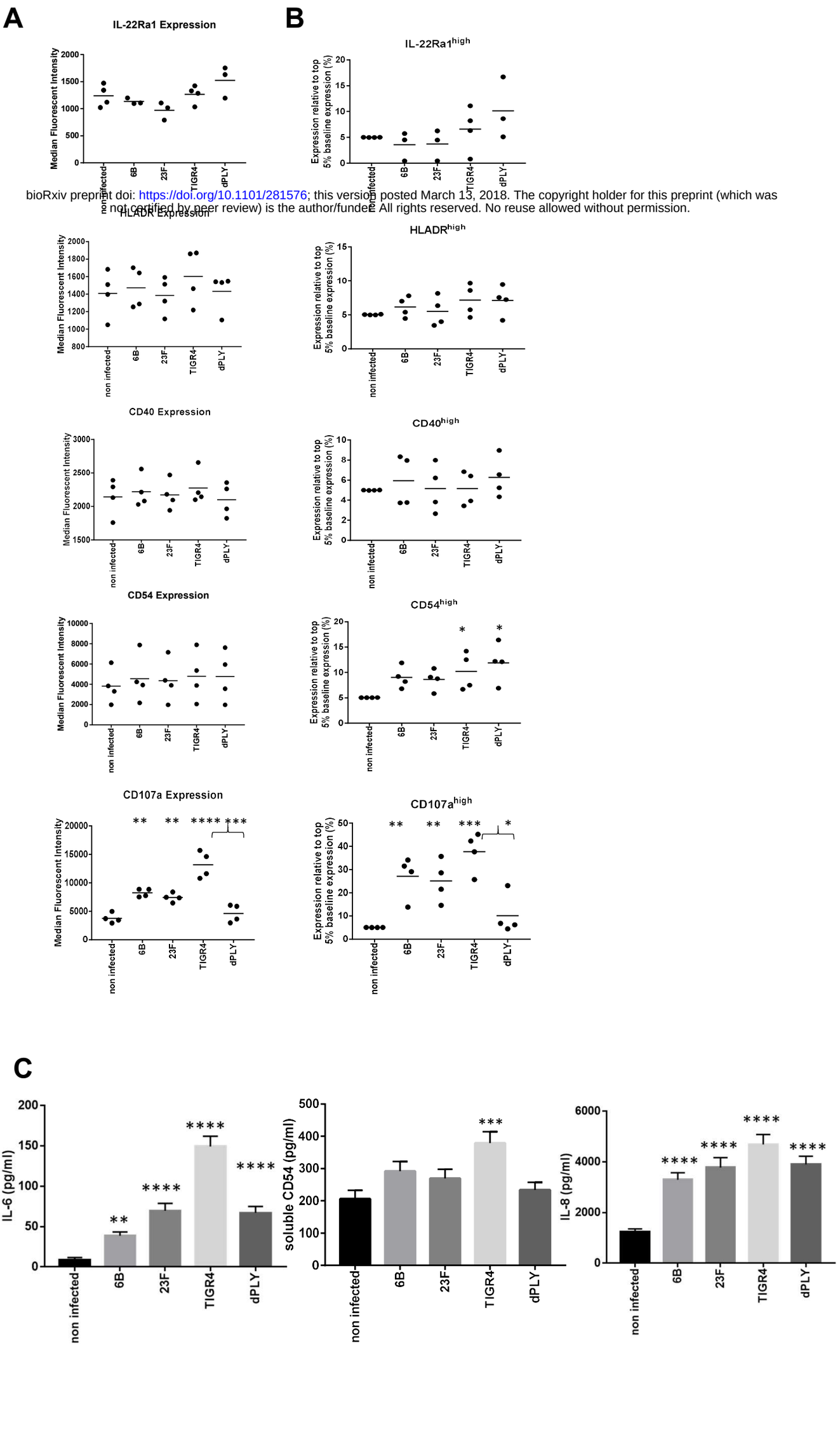

Figure 5

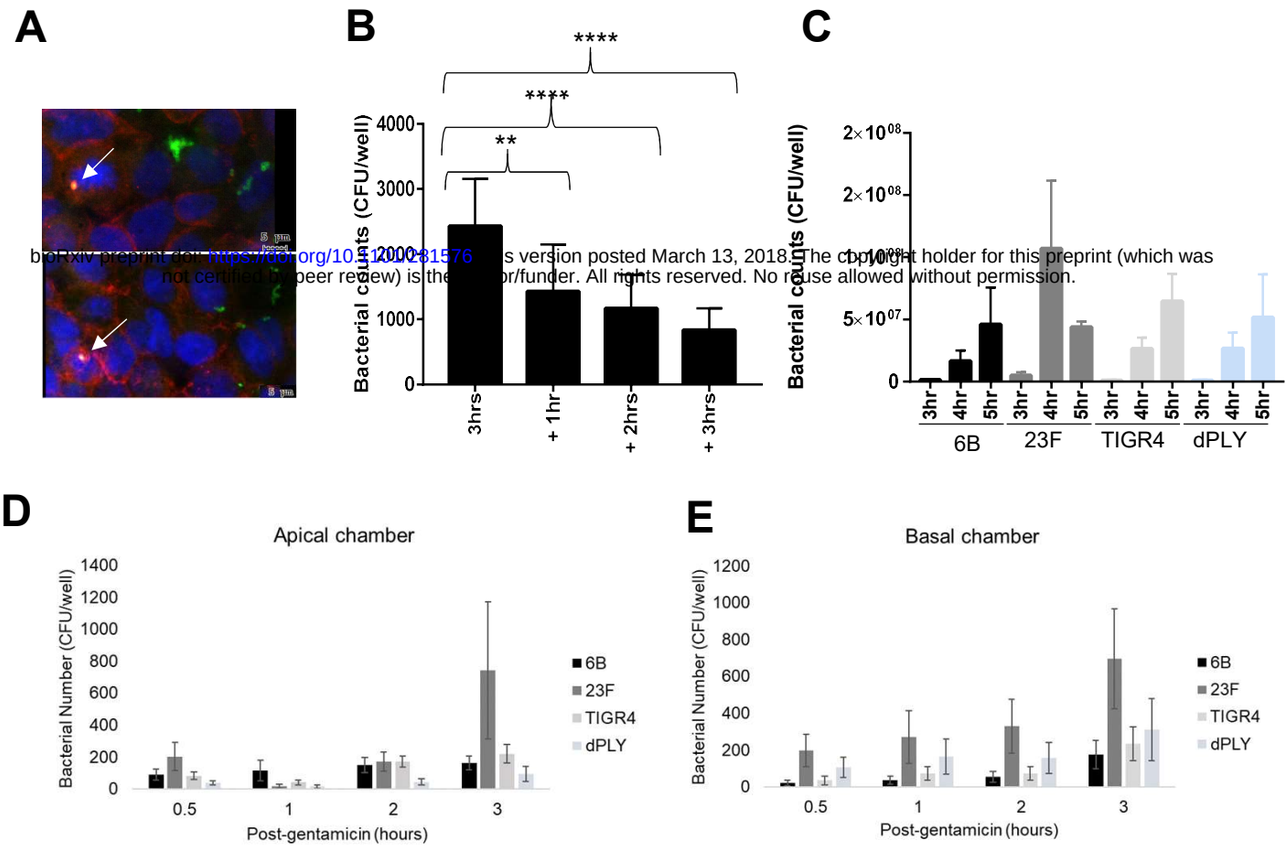

Figure 6

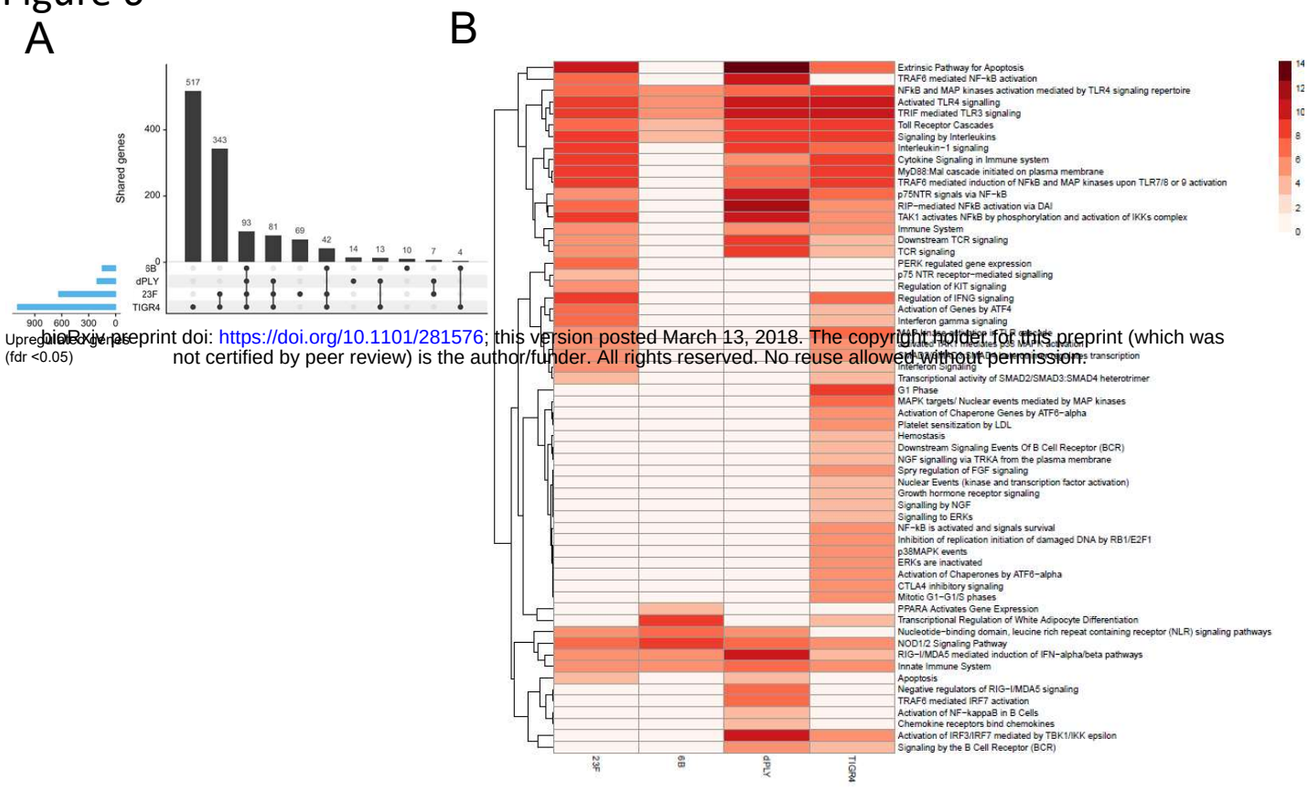

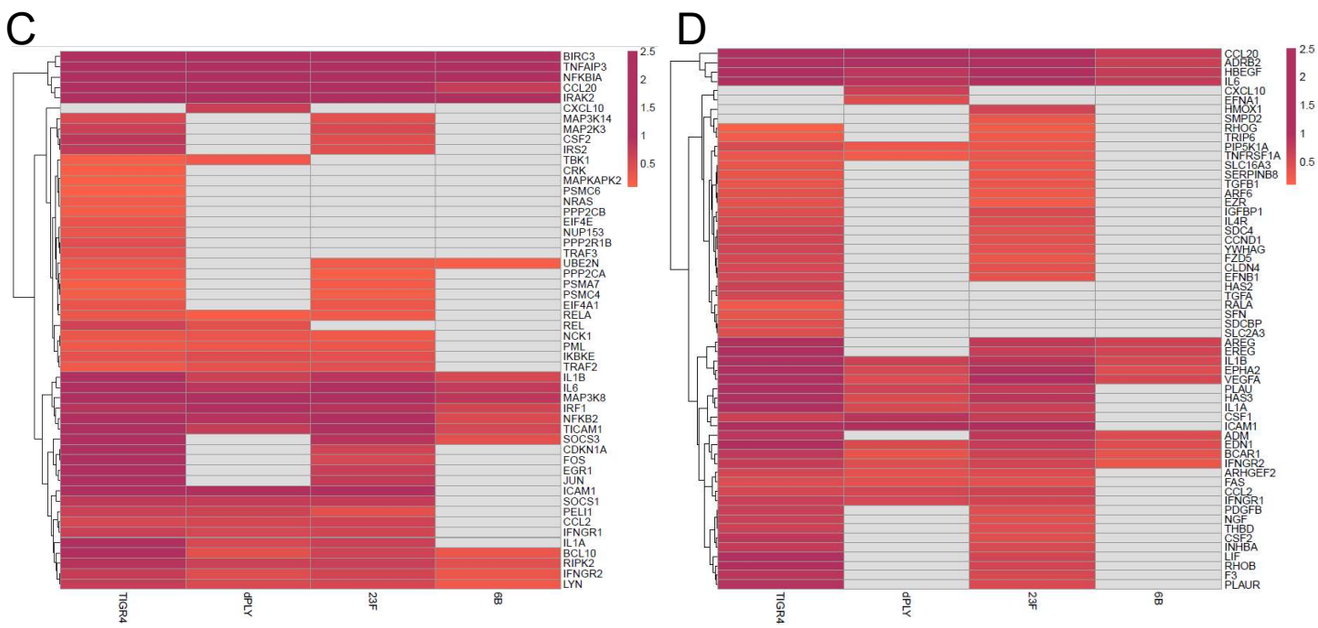

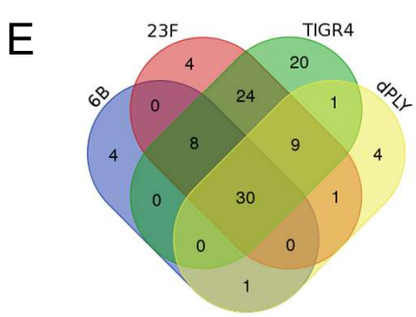

Transcription Factor				
6B, 23F, TIGR4, dPLY	**6B**	**23F**	**TIGR4**	**dPLY**
ECSIT	TCF4	WT1	ETS1	PSMD10
NFKBIA	EIF4E	NCOA3	ATF7	IRF5
IFI16	ZBTB17	FOXO3	FLI1	NFKBIB
JUNB	CCND1	RUNX2	NCOA1	IRF7
ATF4			NOTCH1	
SMARCA4			SMARCB1	
STAT3			SREBF1	
FOXL2			ETV4	
FOXO1			MED1	
NUPR1			TARDBP	
RELA			ELF3	
HIF1A			SREBF2	
NFATC1			SMAD2	
TGIF1			XBP1	
TP53			Gm21596/Hmgb1	
STAT1			MYC	
REL			ETV1	
POU5F1			ARNT2	
TP63			TEAD1	
EGR1			MYB	
CTNNB1				
NFATC2				
NFKB1				
BCL10				
JUN				
STAT4				
HMGB1				
PPRC1				
EZH2				
CREB1				

Figure 7

A

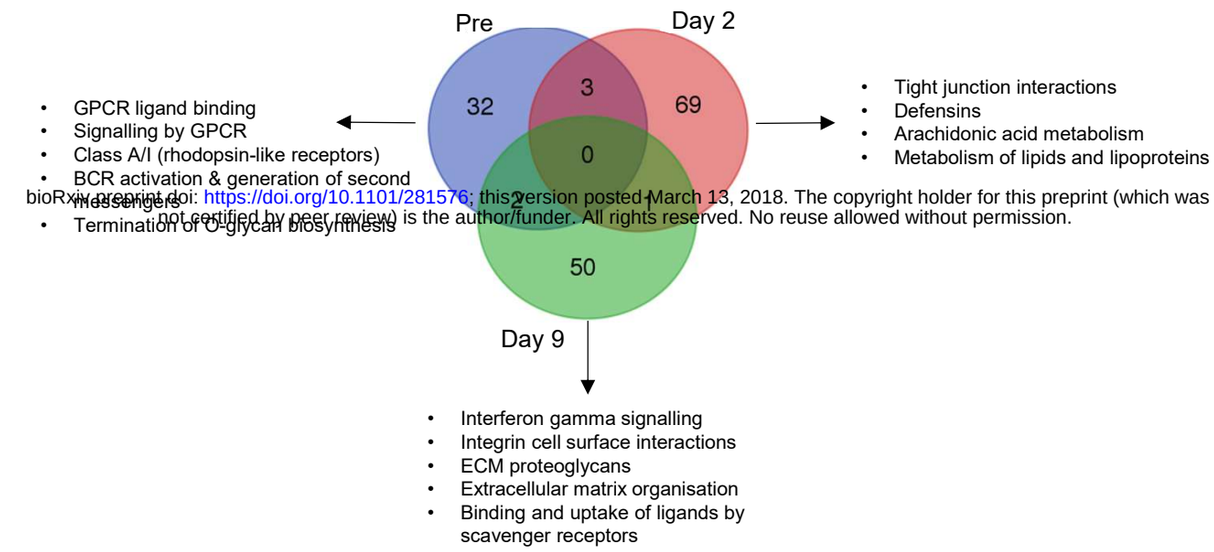

B

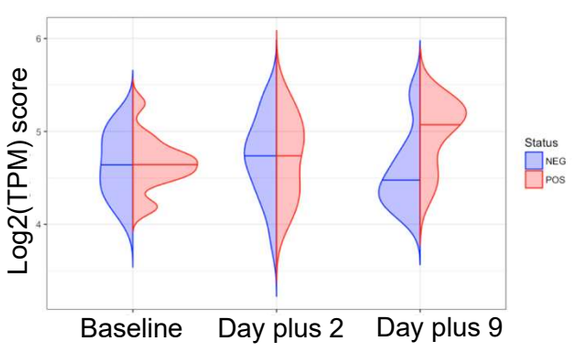

C

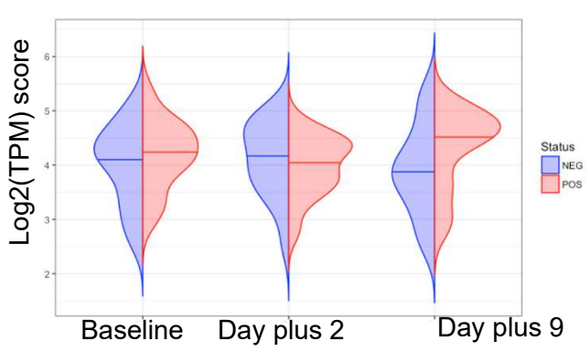

Figure 8